Conformal thin-sandwich solver for generic initial data

William E. East, Fethi M. Ramazanoğlu, and Frans Pretorius

Department of Physics, Princeton University, Princeton, New Jersey 08544, USA
(Received 17 August 2012; published 27 November 2012)

We present a new scheme for constructing initial data for the Einstein field equations using the conformal thin-sandwich formulation that does not assume conformal flatness or approximate Killing vectors. This includes a method for determining free data based on superposition, as well as a way to handle black hole singularities without excision. We numerically solve the constraint equations using a multigrid algorithm with mesh refinement. We demonstrate the efficacy of the method with initial data solutions for several applications: a quasicircular binary black hole merger, a dynamical capture black hole-neutron star merger, and an ultrarelativistic collision.

I. INTRODUCTION

The purview of numerical relativity has extended to include not only relativity theory but also a wide range of other topics. Motivated by current and upcoming efforts to detect gravitational waves [1–5], there has been extensive work on mergers of binary compact objects [6] including binary black holes (BH-BH) [7–10], binary neutron stars, and black hole-neutron star (BH-NS) systems [12,13]. In addition to binaries in quasicircular orbits, there have also been studies of eccentric binaries [14–24] as may arise, for example, from dynamical capture. Other works of interest to astrophysics include gravitational collapse of stars [25,26], black hole accretion [27], and the nature of cosmological singularities [28,29]. Aside from astrophysical systems, numerical relativity has also emerged as a useful tool to explore various concepts in gravity and high energy physics [30], such as critical collapse [31], ultrarelativistic collisions [32–36], the gauge/gravity duality [37–41], gravity and black holes in higher dimensions [42–44], and the (in)stability of anti-de Sitter spacetime [45]. In all these applications, a necessary ingredient is a good method for constructing initial data (ID). Here we present a new initial data solver, based on the conformal thin-sandwich (CTS) [46] formulation, which we have designed to be more generally applicable to a range of physical scenarios by avoiding symmetry or simplifying assumptions.

There has been extensive research on the problem of constructing ID for general relativity, and detailed reviews can be found in Refs. [47–50]. Early attempts at solving the initial data problem relied on certain assumptions to make the mathematical formulation of the problem more tractable, such as conformal flatness and maximal slicing. The widely used Bowen-York solution [51] is one such example. These assumptions are restrictive since, for example, the isolated Kerr black hole does not admit conformally flat slices [52], and consequently the Bowen-York solution cannot be used to construct black holes with spin higher than $S/M_{\mathrm{ADM}}^2 = 0.928$ [53,54]. Other examples include the use of quasiequilibrium assumptions

for constructing ID for binary systems (such as approximate helical Killing vectors or the like, and approximate hydrostatic equilibrium for any matter in the system); see, for example, Refs. [55–70]. This serves as a good approximation for astrophysically motivated quasicircular inspiral sufficiently far from merger, though it is not valid for eccentric mergers (except possibly near the turning points of the orbit [71]) or the ultrarelativistic scattering problem. Many of these studies made further simplifying assumptions, such as conformal flatness, which does not have an astrophysical motivation. Attempts to supply more realistic conformal initial data include superposition of isolated black hole spacetimes [54,72–77], and in addition using post-Newtonian solutions [78,79] and matched asymptotic expansions to supply an initial outgoing radiation field [80–82]. Using superposed data allowed evolution of binary black holes in quasicircular orbits with spins exceeding the Bowen-York limit [83]. A further alternative approach, initially applied to binaries including neutron stars, involves solving the full Einstein-Euler system of equations with a waveless and/or near-zone helical symmetry approximation [67,84–87].

Since our goal is to have a more general purpose numerical initial data solver that can be used for a range of applications, as outlined in the first paragraph, we will use the CTS formalism with arbitrary conformal metric and other free data to be chosen as needed for the particular application. For our first version of the code, as presented here, we restrict to four-dimensional, asymptotically flat spacetimes, with application to binary compact object interactions. For the free data we use superposed, boosted single CO spacetimes. At large separation this is a good approximation for the physical metric of dynamical capture binaries and the ultrarelativistic scattering problem, and the nonlinear corrections from solving the CTS equations are small. For quasicircular binaries, again at large separation this is a good approximation. However, unlike the scattering problems, at practical (because of limited computational resources) initial separations to allow evolution through merger, the simple superposition we use at present

will not give improved astrophysically relevant ID compared to current quasiequilibrium approaches. Compared to existing studies using superposed data, a couple of novel aspects about our work is we include the matter and metric in the superposition of COs involving fluid stars (as opposed to solving the Euler equations on a flat background in the studies mentioned earlier, or conformal to a single black hole solution [69]) and the consideration of ultrarelativistic initial boosts with Lorentz factors up to 10.

Another notable aspect of this work is how we handle black hole singularities. Most existing approaches either use some form of boundary condition on a trapped surface on or inside each black hole (see, for example, Refs. [47,55,64]) or use a slice that maps the interior region of the computational domain for each black hole to either part (so-called "trumpets" [88–91]) or all ("punctures" [92]) of a different asymptotically flat region spanned by an Einstein-Rosen bridge (for a novel variant that does not require separation of the metric into a background piece and conformal factor see Ref. [93]). Here we follow an alternative approach where some distance inside the apparent horizon of each black hole we replace the vacuum interior with an (unphysical) distribution of stress energy to regularize the interior metric. This is similar to a "stuffed black hole" [94] or the "turduckening" evolution scheme [95,96] (see also Ref. [97]). However, since we use excision to subsequently evolve the initial data, with the excision surface chosen to entirely contain the unphysical matter, here it is merely a device to set up a simple initial data problem without explicit interior boundary conditions or singularities. Note, however, that if we were to solve the ID on a domain with traditional excision surfaces inside each black hole, we would (assuming a well-posed elliptic problem) obtain the same solution exterior with appropriate excision boundary conditions, though the mapping between some unphysical interior and appropriate boundary conditions would be nontrivial and in general nonunique.

An outline of the rest of the paper is as follows. In Sec. II we review the CTS formulation, describe our method for choosing the metric and fluid free data, outline the scheme for regularizing black hole solutions, and describe how we numerically solve the constraint equations using a multigrid solver. In Sec. III we present examples of initial data obtained with our solver for quasicircular, eccentric, and ultrarelativistic mergers of compact objects. Finally, we comment on our results and discuss possible future improvements in Sec. IV. In the Appendix we give some details on how we treat mesh refinement boundaries in our multigrid algorithm. We use geometric units where Newton's constant $G = 1$ and the speed of light $c = 1$.

II. COMPUTATIONAL METHODOLOGY

A. Conformal thin-sandwich equations

To formulate the initial data problem for general relativity, we start by foliating spacetime with a family of spacelike hypersurfaces Σ_t parametrized by t. The normal vector to these surfaces n^μ and the generator of time translations t^μ satisfy

$$t^\mu = \alpha n^\mu + \beta^\mu, \tag{1}$$

where α is the lapse and β^μ is the shift, which is tangent to Σ_t ($n_\mu \beta^\mu = 0$). We use the standard convention where Greek indices run through $\{0, 1, 2, 3\}$ and represent the full spacetime coordinates, while Latin indices run through $\{1, 2, 3\}$ and represent coordinates intrinsic to a given spatial hypersurface. Using the orthogonal projection operator $\perp^\mu{}_\nu \equiv \delta^\mu{}_\nu + n^\mu n_\nu$, we obtain the induced metric on Σ_t, $\gamma_{ij} \equiv g_{\mu\nu} \perp^\mu{}_i \perp^\nu{}_j$, where $g_{\mu\nu}$ is the four-dimensional spacetime metric. The line element can be written in terms of these quantities as

$$ds^2 = -\alpha^2 dt^2 + \gamma_{ij}(dx^i + \beta^i dt)(dx^j + \beta^j dt). \tag{2}$$

The extrinsic curvature of a slice Σ_t can be written in terms of a Lie derivative as

$$K_{ij} \equiv -\frac{1}{2}\mathcal{L}_{\mathbf{n}}\gamma_{ij}. \tag{3}$$

Projecting the Einstein equations onto the hypersurface Σ_t, one obtains the constraint equations

$$R + K^2 + K_{ij}K^{ij} = 16\pi E, \tag{4}$$

$$D_j K^{ij} - D^i K = 8\pi p^i, \tag{5}$$

where $K = \gamma^{ij}K_{ij}$, R, and D_i are the Ricci scalar and covariant derivative associated with γ_{ij}, respectively, and E and p^i are the energy and momentum density as measured by an Eulerian observer, respectively.

In the language of the $3 + 1$ decomposition, initial data for the Einstein field equations (and any matter evolution equations) are a set of 20 functions representing the components of α, β^i, γ_{ij}, K_{ij}, E, and p^i on the initial slice Σ_t that together satisfy the constraints (4) and (5). Though, in principle, there are numerous conceivable ways of coming up with consistent initial data, it is challenging to separate freely specifiable versus constrained degrees of freedom in a manner where the underlying physical interpretation of the free data is transparent, and where the choice of the free data leads to a well-posed set of constraint equations. The CTS method [46] is a prescription for this separation of degrees of freedom that begins with a conformal decomposition of the spatial metric and the extrinsic curvature. Introducing the conformal factor Ψ, we define

$$\tilde{\gamma}_{ij} \equiv \Psi^{-4}\gamma_{ij}, \tag{6}$$

$$\begin{aligned}\hat{A}^{ij} &\equiv \Psi^{10}\left(K^{ij} - \frac{1}{3}K\gamma^{ij}\right) \\ &= \frac{1}{2\tilde{\alpha}}\left[\dot{\tilde{\gamma}}^{ij} + \tilde{D}^i\beta^j + \tilde{D}^j\beta^i - \frac{2}{3}\tilde{\gamma}^{ij}\tilde{D}_k\beta^k\right],\end{aligned} \tag{7}$$

where $\dot{\tilde{\gamma}}^{ij} \equiv \Psi^4(\dot{\gamma}^{ij} - \frac{1}{3}\gamma^{ij}\gamma_{kl}\dot{\gamma}^{kl})$ is defined to be trace-less, the overdot indicates a time derivative, $\tilde{\alpha} \equiv \Psi^{-6}\alpha$, and $\tilde{R}$ and $\tilde{D}_i$ are the Ricci scalar and covariant derivative associated with $\tilde{\gamma}_{ij}$, respectively. With these definitions we can rewrite (4) and (5) in the CTS form as

$$\tilde{D}_i\tilde{D}^i\Psi - \frac{\tilde{R}}{8}\Psi + \frac{1}{8}\hat{A}_{ij}\hat{A}^{ij}\Psi^{-7} - \frac{K^2}{12}\Psi^5 = -2\pi\Psi^{-3}\tilde{E},$$
(8)

$$\tilde{D}_j\hat{A}^{ij} - \frac{2}{3}\Psi^6\tilde{D}^iK = 8\pi\tilde{p}^i,$$
(9)

with $\tilde{p}^i \equiv \Psi^{10}p^i$, $\tilde{E} \equiv \Psi^8 E$. Initial data are obtained by solving this system of four elliptic equations for Ψ and β^i [upon substitution of (7) into (9)], where $\tilde{\gamma}_{ij}$, $\dot{\tilde{\gamma}}^{ij}$, K, $\tilde{\alpha}$, $\tilde{E}$, and $\tilde{p}^i$ are the "free data" that can be freely specified to reflect the physical system under investigation.

B. Superposed free data

Under the conformal thin-sandwich method one is free to choose any values for $\tilde{\gamma}_{ij}$, $\dot{\tilde{\gamma}}^{ij}$, $\tilde{\alpha}$, K, $\tilde{E}$, and $\tilde{p}^i$ for which a solution can be found. In this section we outline our method for determining these free data in order to construct initial data representing binary systems. The basic idea is as follows. Since solutions to the Einstein equations representing isolated compact objects (black holes, stars, etc.) are well known, and since if the separation between the objects is not too small the solution describing two compact objects is well-approximated by superposing the two isolated solutions, we therefore set our free data using such a superposed solution and then solve the constraint equations in order to obtain the nonlinear correction.

There are many ways to combine the metrics representing isolated compact objects. The method we use is based on the 3 + 1 splitting. Let $\gamma_{ij}^{(1)}$, $\dot{\gamma}_{ij}^{(1)}$, $\alpha^{(1)}$, and $\beta^{i(1)}$ represent the spatial metric, time derivative of the spatial metric, lapse, and shift, respectively, of the first isolated solution (e.g., a boosted black hole or neutron star solution) and similarly for the second isolated solution. Then, we construct the following quantities:

$$\gamma_{ij}^{(\text{sup})} = \gamma_{ij}^{(1)} + \gamma_{ij}^{(2)} - f_{ij},$$
(10)

$$\dot{\gamma}_{ij}^{(\text{sup})} = \dot{\gamma}_{ij}^{(1)} + \dot{\gamma}_{ij}^{(2)},$$
(11)

$$\alpha^{(\text{sup})} = \alpha^{(1)} + \alpha^{(2)} - 1,$$
(12)

$$\beta^{i(\text{sup})} = \beta^{i(1)} + \beta^{i(2)},$$
(13)

where f_{ij} is the flat-space metric. This particular construction will break down if $\alpha^{(\text{sup})} \leq 0$ or $\det[\gamma_{ij}^{(\text{sup})}] \leq 0$ anywhere in the domain, which would then require some other way of combining the metrics, for example, using distance-weighted attenuation functions as in Ref. [98]. (In Ref. [76]

it was also found necessary to enforce a desired asymptotic falloff of the superposed metric, owing to the use of a corotating frame.) However, these conditions are not violated for the cases considered here. From the above quantities, we then calculate the free data we will use when solving the CTS equations from the usual relations:

$$\tilde{\gamma}_{ij} = \gamma_{ij}^{(\text{sup})},$$
(14)

$$\dot{\tilde{\gamma}}^{ij} = -\tilde{\gamma}^{ik}\tilde{\gamma}^{jl}\left(\dot{\gamma}_{kl}^{(\text{sup})} - \frac{1}{3}\tilde{\gamma}^{mn}\dot{\gamma}_{mn}^{(\text{sup})}\tilde{\gamma}_{kl}\right),$$
(15)

$$\tilde{\alpha} = \alpha^{(\text{sup})},$$
(16)

$$K = \frac{1}{2\tilde{\alpha}}(2\partial_i\beta^{i(\text{sup})} + \dot{\tilde{\gamma}}^{ij}\tilde{\gamma}_{ij} + \tilde{\gamma}^{ij}\beta^{k(\text{sup})}\partial_k\tilde{\gamma}_{ij}).$$
(17)

For initial data with matter we use a similar method. We set $\tilde{E}$ and $\tilde{p}^i$ by superposing the energy and momentum density of the two objects (we do not consider situations where they would both be nonzero at the same point). For some cases (in particular for the ultrarelativistic boosts), we rescale the momentum density so that its magnitude with respect to the superposed metric $\tilde{\gamma}_{ij}$ is equal to the magnitude of the original momentum density with respect to the metric of the isolated object ($\gamma_{ij}^{(1)}$ or $\gamma_{ij}^{(2)}$). This ensures that $\tilde{E}^2$ and $\tilde{p}^i\tilde{p}_i$ have the same ratio as the isolated objects. This is important since the choice of conformal scaling of the energy $\tilde{E} = E\Psi^8$ was designed to ensure that if the conformal quantities satisfy the dominant energy condition, $\sqrt{\tilde{\gamma}_{ij}\tilde{p}^i\tilde{p}^j} \leq \tilde{E}$, then so will the rescaled quantities following the solution of the constraints.

C. Regularizing black hole solutions

In cases where black holes are a part of the physical system, the divergences at the black hole's singularity must be addressed. As discussed in the Introduction, there are several ways to deal with this issue in the initial data problem; the approach we take here is to explicitly modify the metric of an isolated (prior to superposition) black hole solution inside the horizon to take a prescribed, regular form. The regularized region will not in general satisfy the vacuum constraint equations, and to avoid a singular conformal factor and shift vector components when solving the constraints with such background data, we introduce unphysical energy momentum in the union of black hole interiors so that these regions automatically satisfy the constraints, albeit with the unphysical interior matter source.

We start with a single, unboosted spinning black hole spacetime in horizon penetrating coordinates (for the results described here we use the harmonic form of Kerr derived in Ref. [99], though we have also tried it using Kerr-Schild coordinates without difficulty), so that the only divergences in the metric components are well within the

horizon. We then choose a surface that encloses the singular region, yet is strictly inside the event horizon. The interior of this surface we call the *regularization region.* Outside the regularization region we do not modify the metric. Inside, there are many conceivable ways to alter the metric to eliminate the divergences. The simple approach we take is to promote the black hole mass M and spin a constants to functions of space and smoothly decrease them from their bare values at the regularization surface to zero at some surface interior to this.

Specifically, we introduce a regularization function

$$f_{\text{reg}}(x) = \begin{cases} 1, & x > 1, \\ x^3(6x^2 - 15x + 10), & 1 > x > 0, \\ 0, & 0 > x, \end{cases} \quad (18)$$

chosen to be twice continuously differentiable so that the consequent unphysical energy is well behaved. We use a Cartesian grid[1] and define $r^{(E)}(x, y, z) = \sqrt{x^2 + y^2 + z^2}$ as the Euclidean radius for a point with coordinates x, y, z. We then replace the mass M and the spin parameter a with $\xi(x, y, z)M$ and $\xi(x, y, z)a$, respectively, in all the metric components, where

$$\xi(x, y, z) = f_{\text{reg}}\left(\frac{(r^{(E)}(x, y, z)/r_+^{(E)}(x, y, z)) - q_{\text{in}}}{q_{\text{out}} - q_{\text{in}}}\right), \quad (19)$$

$r_+^{(E)}(x, y, z)$ is the Euclidean radius for the point on the event horizon at the same angular direction as (x, y, z), q_{out} defines the outer surface of the regularization region, and q_{in} is the inner surface inside of which the metric is Minkowski, with $1 > q_{\text{out}} > q_{\text{in}} > 0$. The shape of the regularization region, namely a shrunken form of the interior of the event horizon, was motivated by the similar volume excised during evolution (though that is based on the apparent horizon, and the excision surface is a best-fit ellipsoid rather than the exact shape of the apparent horizon). The particular values of q_{out} and q_{in} are not too important (i.e., give essentially the same solutions), the only practical requirements being that q_{out} represents a surface within the excision surface we will use during evolution and that q_{in} is not to be too close to q_{out}; otherwise excessive resolution is needed to resolve the transition.

Once we have an everywhere-regular metric, we superpose it with any other COs to construct the free data as described in Sec. II B. We then compute the unphysical energy and momentum we will add to the regularization regions simply by evaluating (4) and (5) with the background, superposed data

---

[1]Note that in the harmonic coordinates of Ref. [99] only the region with $r_K > M$ is represented on the Cartesian grid $r \geqq 0$, where r_K is the radial coordinate of the the metric in ingoing null Kerr form. Hence the physical singularity is not on the grid; however, the metric components are discontinuous at $x = y = z = 0$ ($r_K = M$), and hence regularization is still required.

$$E_{\text{unphys}} \equiv \frac{1}{16\pi}(R + K^2 + K_{ij}K^{ij})^{(\text{sup})}, \quad (20)$$

$$p_{\text{unphys}}^i \equiv \frac{1}{8\pi}(D_j K^{ij} - D^i K)^{(\text{sup})}. \quad (21)$$

E_{unphys} and p_{unphys}^i are then added to $\tilde{E}$ and $\tilde{p}^i$ within the regularization regions, and we can then solve the CTS equations as usual without any additional special treatment of these regions. It is also possible to calculate the unphysical energy momentum before the superposition and add E_{unphys} and p_{unphys}^i directly. The former method gives a small discontinuity of E_{unphys} and p_{unphys}^i at the boundary of the regularization region, whereas the latter one gives continuous quantities. Either approach leads to similar results, but the former gives more rapid relaxation of the elliptic equations and is the choice for the cases presented here.

During evolution, we choose black hole excision surfaces that entirely contain the regularization regions and unphysical matter. Thus, one can think of the unphysical matter as serving as a proxy for what would otherwise be boundary conditions for Ψ and β^i on excision surfaces. Given a solution to the constraints with regularized interiors, it is trivial to read off what the equivalent (Dirichlet) boundary conditions would have been, though the inverse problem of mapping some set of desired boundary conditions to interior sources is less trivial and likely not well posed in general.

D. Fluid solutions

For the applications with (physical) matter considered here we use Tolman-Oppenheimer-Volkov (TOV) star solutions in isotropic coordinates to construct the metric free data quantities as well as $\tilde{E}$ and $\tilde{p}^i$. Such solutions are derived by assuming a relationship between the pressure and density $P(\rho)$, e.g., as given by a polytropic condition. Once the constraint equations have been solved and E and p^i found, we determine the new density and pressure profiles using this same relationship and solving the equation

$$(E + P(\rho))(E - \rho) - p_i p^i = 0, \quad (22)$$

for ρ, which follows directly from the expressions for the energy and momentum density of a perfect fluid. For the applications considered here, we do not explicitly impose any additional constraints on the fluid quantities (e.g., that the fluid be in hydrostatic equilibrium). We leave that to future extensions.

E. Multigrid elliptic solver

To numerically solve the CTS equations we discretize (8) and (9) using standard second-order finite difference operators and solve them using a full approximation storage implementation of the multigrid algorithm with adaptive mesh refinement (AMR) as described in

Ref. [100]. A multigrid algorithm is characterized by a smoothing operation and by a choice of restriction and prolongation operators. We use Newton-Gauss-Seidel relaxation for smoothing, and half-weight restriction and linear interpolation for the restriction and prolongation operators, respectively. These latter operators require special treatment on mesh refinement boundaries, which we outline in the Appendix. Unlike in the evolution code, we do not use a compactified coordinate system extending to spatial infinity. Rather, the initial data numerical grid extends to a large but finite radius. This is to avoid numerical problems attributable to large Jacobian factors needed in compactification, which become especially problematic near the corners of the boundary. At the outer boundaries we impose boundary conditions that $\Psi = 1$ and $\beta^i = \beta^{i(\text{sup})}$. Since the use of mesh refinement enables us to put the outer boundary far away from the compact objects, these boundary conditions can be made sufficiently accurate compared to numerical error (though for future applications they could also be replaced with, e.g., Robin boundary conditions). Any points outside this domain on the evolution grid are initialized via extrapolation, assuming a leading order $1/r$ approach to an asymptotically flat spacetime.

For some applications we wish to solve for initial data with axisymmetry. To efficiently solve the constraint equations in these situations, we have implemented a modified version of the Cartoon method [101] similar to that used in Ref. [102]. Letting the y axis be the axis of symmetry, we restrict our computational domain to a subset of the half-plane $(x, y) \in (-\infty, \infty) \times [0, \infty)$. We use the existence of an axisymmetric Killing vector to express derivatives in the z direction in terms of derivatives in the x and y directions. On the y axis we impose regularity, which gives the following conditions for the constrained variables: $\partial_y \Psi = 0$ and $\partial_y \beta^x = \partial_y \beta^y = \beta^z = 0$.

III. APPLICATIONS

A. Quasicircular binary black holes

As a first application of our technique, we generate and evolve ID for the (approximate) quasicircular inspiral of two nonspinning, equal-mass black holes. Our present method for providing free data is not designed to easily give initial data for quasicircular inspiral (though presumably with sufficient fine-tuning of the boost vectors this could be achieved), and this basic example is mainly to provide a relatively low eccentricity binary, a couple of orbits before merger, for comparison to past studies. Specifically, we are interested in seeing how close the masses, etc., of the black holes obtained following the solution of the constraints are to the corresponding parameters used in constructing the free data, and how much ''spurious'' gravitational radiation is present in the initial data.

For the initial data, we use free data set by superposing two boosted nonspinning equal mass black holes at a coordinate separation of $10M$, where M is the sum of the isolated black hole masses (which in general will be different from the irreducible masses of the black holes once the constraint equations are solved). The black holes are given purely tangential boost velocities chosen so that, when evolved, the black holes undergo a few orbits with monotonically decreasing proper separation. The initial data grid extends to $\pm 2048M$ in all three directions. For convergence studies of the initial data solver, we use three base grid sizes of 33^3, 65^3, and 129^3 and 12 levels of mesh refinement with identical grid structures in each case. As expected, the conformal factor and shift vector exhibit second-order convergence as shown in Figs. 1 and 2, as does the residual of (4) and (5). For evolution, we use the highest resolution initial data. The ID is evolved using the generalized harmonic formulation of the field equations, choosing harmonic coordinates at $t = 0$ and transitioning to a damped harmonic gauge as described in Ref. [103]. The eccentricity is estimated to be $e \approx 0.05$ based on the evolution of the coordinate distance between the centers of the apparent horizons as shown in Fig. 3. Though the orbital eccentricity could presumably be reduced further by tuning the initial velocities using methods such as the one proposed in Ref. [104] or using the post-Newtonian approximation as in Ref. [105], we did not attempt to do so for this basic comparison. Because of corrections from solving the constraints, the sum of the masses of the isolated black holes whose spacetimes we superpose M is different from the sum of irreducible masses
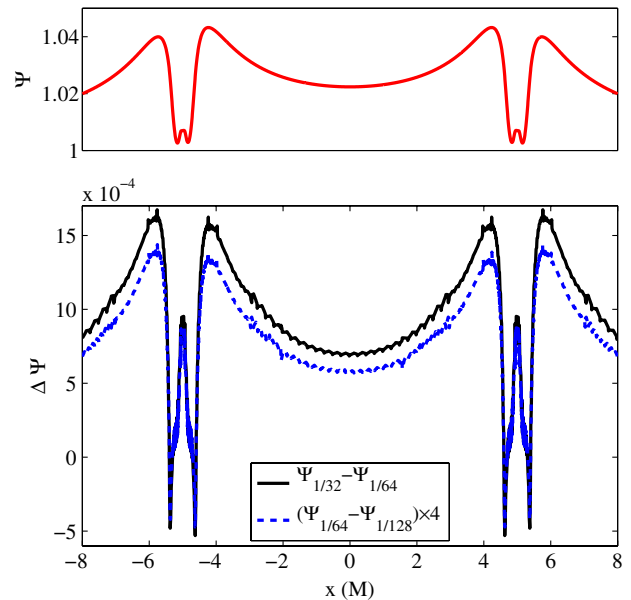

FIG. 1 (color online). The conformal factor Ψ from BH-BH ID. Upper: Ψ on the x axis, which lies on the orbital plane and goes through the centers of the black holes. Lower: Differences in Ψ with resolution on the x axis, scaled assuming second-order convergence.
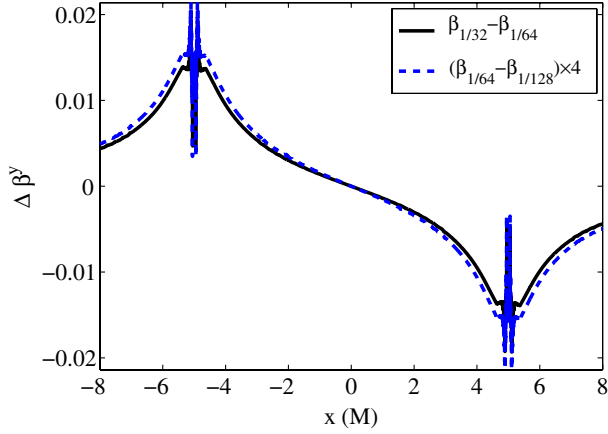
FIG. 2 (color online). Differences in the shift component β^y with resolution on the x axis from BH-BH ID, scaled assuming second-order convergence.

FIG. 4 (color online). The real and imaginary components of the $l = 2$, $m = 2$ spin-weight -2 spherical harmonic of $r\Psi_4$ extracted at a radius of $105M$. Time is measured from the beginning of the simulation.

computed from their apparent horizons at the beginning of the evolution $M_{\rm irr}$. For this particular case $M_{\rm irr}/M = 1.21$. The ID is constructed using free data with nonspinning black holes, and the initial spin calculated from the apparent horizons is zero to within truncation error ($|S/M_{\rm BH}^2| < 6 \times 10^{-3}$). The ratio of the irreducible mass of the final black hole after the merger to the sum of the irreducible masses of the initial black holes is $M_{{\rm irr},f}/M_{\rm irr} = 0.885$, and the dimensionless spin parameter of the final black hole is $a_f/M_f = 0.678$. Both of these values are in good agreement (considering the mild initial eccentricity here) with the high accuracy results of 0.88433 and 0.68646, respectively, from Ref. [106]. In Fig. 4 we show the gravitational waves from the BH-BH merger. The initial spurious part of the
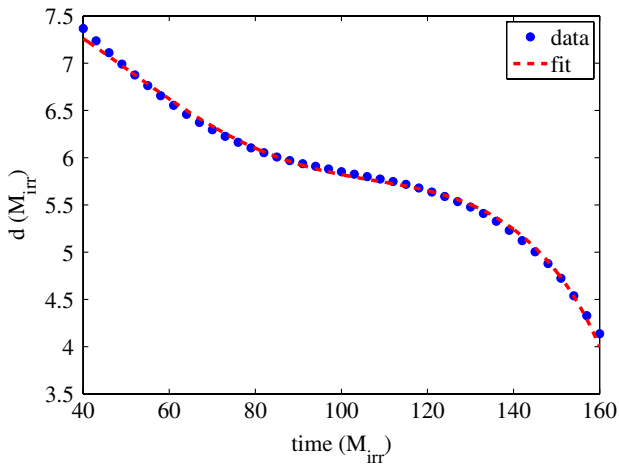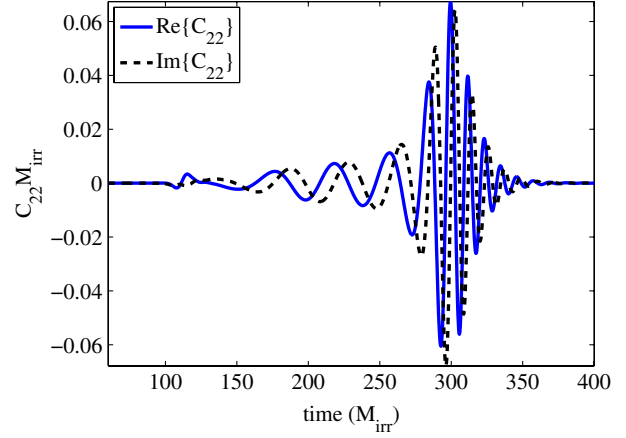
signal is of comparable magnitude to other ID approaches that do not attempt to include gravitational waves from the prior inspiral; see, for example, Ref. [82].

B. Eccentric compact object mergers

As another application of this technique, we consider constructing initial data describing a dynamical capture BH-NS binary. We set the free data using a boosted harmonic black hole solution and a neutron star with the equation of state labelled HB in Ref. [107]. Let M be the sum of the masses of the isolated black hole and neutron star. We construct initial data for a 4:1 BH-NS binary by setting the boost velocities to correspond to a Newtonian orbit with eccentricity $e = 1$ and periapse distance $r_p = 5M$ at various initial separations d. We keep the mass and spin that we use for the black hole component of the free data fixed at $0.8M$ and $-0.4M$, respectively (where the negative sign indicates that the spin is retrograde with respect to the orbital angular momentum), and the mass of the neutron star component of the free data fixed at $0.2M$. The spin and masses will receive corrections from solving the constraint equations, and with decreasing d these will differ more and more from the input parameters of the free data. The input parameters can, of course, be tuned to achieve desired values in the final solution. However, since here we are mainly interested in quantifying this difference, we keep them fixed. We use a grid extending from $-1600M$ to $1600M$ in each dimension where the base level is covered by 257^3 points and there are nine additional levels of mesh refinement, each with a refinement ratio of two. We solve for data with initial separations $d/M = 15$, 25, and 50. In Table I we show the maximum difference of the conformal factor from unity as well as the actual ADM (Arnowitt-Deser-Misner) mass, black hole mass and spin, neutron star rest mass, and induced neutron star density oscillations for

FIG. 3 (color online). Coordinate separation of the centers of the two black holes fitted to a function $(A - B(t - t_0))^{1/4} + C\cos(\omega(t - t_0) + \phi)$. This function combines the decaying orbit attributable to quadrupole radiation with the effects of eccentricity, given by $e = C/d(t = t_0) \approx 0.05$. Because of early-time gauge effects (a transition from harmonic to damped harmonic gauge) we exclude the first $t = 40M_{\rm irr}$ from the fit.

TABLE I.   Characteristics of BH-NS initial data with Newtonian orbital parameters $r_p = 5M$ and $e = 1$ with three initial coordinate separations d. Here $\max(|\Psi - 1|)$ is the maximum deviation over the entire domain of the conformal factor from the background free-data value of unity, $M_0/M_{0,\infty}$ is the rest mass of the neutron star compared to its isolated rest mass, M_{BH}/M and a_{BH}/M are the black hole mass and spin parameters measured from the apparent horizon relative to the initial total mass M of the free data, M_{ADM}/M is the relative ADM mass of the solution, and ρ_{oscill} is the relative magnitude of the oscillation in time of the maximum rest-mass density of the neutron star induced by the ID construction.

d/M	$\max(|\Psi - 1|)$	$M_0/M_{0,\infty}$	M_{BH}/M	a_{BH}/M	M_{ADM}/M	ρ_{oscill} (%)
15	0.0155	1.077	0.832	-0.398	1.051	14.3
25	0.0092	1.049	0.818	-0.402	1.030	9.0
50	0.0046	1.028	0.808	-0.399	1.017	4.5

these three different separations. We can see that even at a separation of $15M$ the difference between input and final parameters is small—at the level of a few percent. At such separations, however, the oscillations induced in the neutron star by the initial setup become large. This problem could be remedied by adding additional constraints to the matter, for example, requiring it to satisfy an equilibrium version of the Euler equations.

We evolve the initial data past merger using the same methods, gauge, and three different resolutions as in Ref. [17]. Unless otherwise stated, all quantities are from the high resolution runs. In Fig. 5 we show the norm of the constraints throughout the evolution of the $d = 15M$ ID at the different resolutions. The single highest, resolution ID is used for all evolution runs, so the fact that evolution constraints are converging to zero indicates that the truncation error of the ID is at least as small as that of the highest resolution evolution. In Fig. 6 we plot the

amplitude of the gravitational waves measured from the three different evolutions to show the amount of spurious gravitational radiation this method of constructing ID introduces. The level of spurious gravitational radiation decreases with increasing separation and in all three cases is small—an order of magnitude or more below the physical signal of interest. After the passage of the spurious gravitational radiation, the gravitational wave signal from all three initial separations is approximately the same, though there are small differences owing to the changes in parameters indicated in Table I, and because we are starting the systems along different points of a Newtonian trajectory.

C. Ultrarelativistic initial data

As a final application, we consider the problem of specifying ID for ultrarelativistic collisions. The study of the collision of objects where kinetic energy dominates the dynamics of the spacetime is of considerable interest to
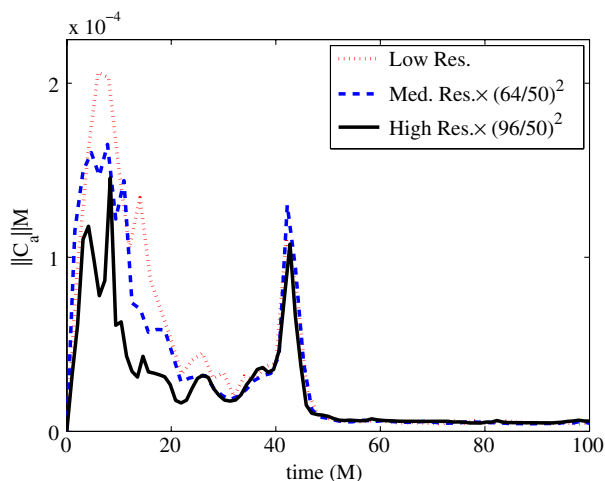

FIG. 5 (color online).   The L^2 norm of the constraint violation, $C_a \equiv H_a - \Box x_a$, in units of $1/M$ for the $d = 15M$ BH-NS merger in the $100M \times 100M$ region around the center of mass in the equatorial plane (i.e., $\sqrt{\int \|C_a\|^2 d^2x / \int d^2x}$). This is shown for low, medium, and high resolutions where the latter two are scaled assuming second-order convergence.

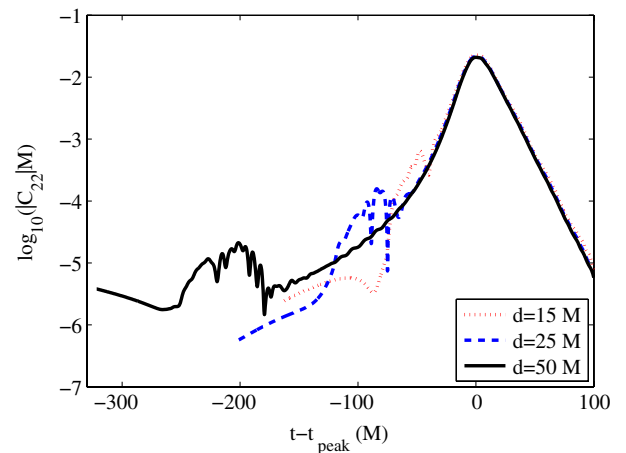

FIG. 6 (color online).   The log of the magnitude of the $l = 2$, $m = 2$ spin-weight -2 spherical harmonic of $r\Psi_4$ for BH-NS simulations with different initial separations d. The value of Ψ_4 was extracted on a sphere of radius $100M$ and is shown starting at the beginning of the simulation and continuing past merger. The waveforms have been aligned so that the peaks occurs at time 0.

super-Planck scale particle collisions, as arguments suggest classical Einstein gravity will be adequate to describe the process [108–110]. The hoop conjecture [111] predicts that the generic outcome of a sufficiently ultrarelativistic collision will be black hole formation, and this, together with suggestions of a tera-electron-volt Planck scale [112,113], imply that, if such a scenario describes nature, the Large Hadron Collider or cosmic ray collisions with Earth could produce black holes [114–116]. Though to date no signs of black hole production have been observed [117,118], the nature of the kinetic energy dominated regime in general relativity is of interest in its own right and has largely been unexplored.

Initial data describing such systems will be far from equilibrium, and one cannot assume that the solution is time symmetric or quasistatic. It is instructive to recall the Aichelburg-Sexl [119] solution describing a gravitational shock wave. The solution can be obtained from a boosted Schwarzschild solution by simultaneously taking the mass to zero and the boost parameter to infinity, while keeping their product constant and finite. Two such oppositely boosted solutions can be superposed to obtain a new solution that is valid up until collision. Though it is not clear how applicable this is to the nonlimiting case, this suggests that superposition may be a good approximation to describing such spacetimes.

Here we consider the specific example of the setup for a head-on collision of two fluid star solutions. We use the method described in Sec. II B to construct free data from two $\Gamma = 2$ polytropic TOV star solutions that have unboosted mass M_* and a compactness (ratio of mass to radius) of $C = 0.01$. The stars are boosted toward each other with boost factor $\gamma = 10$. We consider a sequence of solutions at various initial coordinate separations d. We take advantage of the axisymmetry of the problem and use $[-2000M, 2000M] \times [0, 2000M]$ where $M \equiv 2\gamma M_*$ as our computational domain. The base level is covered by 1025×513 points, and there are nine additional levels of mesh refinement. To test convergence we also consider two lower resolutions with grid spacing 2 and 4/3 times as coarse.

Using the method for specifying free data described in Sec. II B, as $d \rightarrow \infty$ we expect the corrections from solving the constraints will go to zero: $\Psi \rightarrow 1$, the magnitude of the coordinate velocities of the stars $|v|$ will approach $\sqrt{1 - \gamma^{-2}}$, the ADM mass $M_{\rm ADM}$ will approach M, and the total rest mass M_0 will approach the sum of the rest masses of the isolated stars $M_{0,\infty}$. In Fig. 7 we show how all these quantities change with coordinate separation. We can see that it is possible to solve for ID where the stars are quite close together, though the corrections become large, and in particular the ADM mass decreases quite significantly.

To give an indication of the numerical errors on these quantities, we can compare the values obtained at the highest resolution to the Richardson extrapolated values
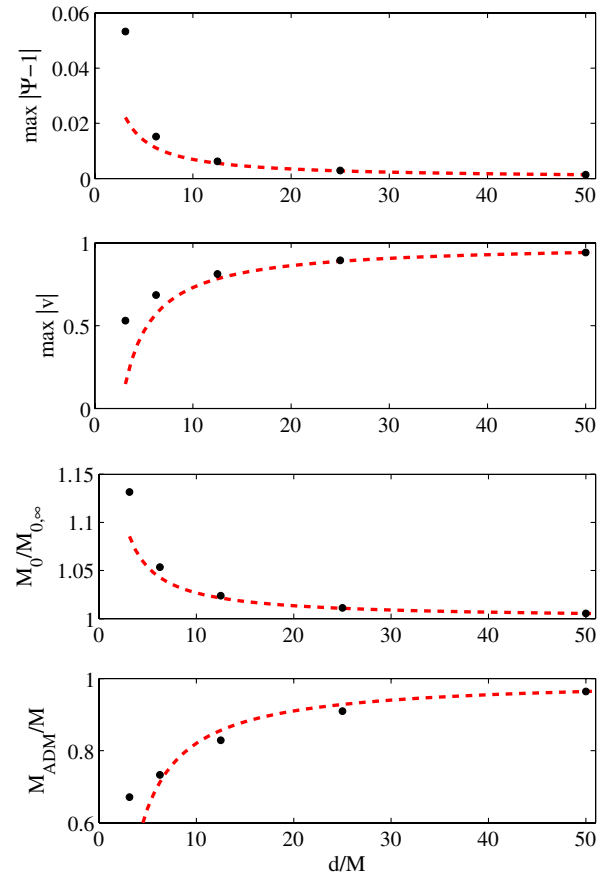

FIG. 7 (color online). Various quantities from ultrarelativistic collision ID with $\gamma = 10$ made using the superposition method for constructing free data. From top to bottom the quantities shown are the maximum (over the entire domain) difference of the conformal factor from unity, the maximum coordinate velocity of the fluid, the total rest mass, and the ADM mass. All quantities are shown as a function of d, the coordinate separation between the two stars. For all these cases the maximum of $|\Psi - 1|$ occurs for values of Ψ that are less than unity. One might expect these quantities to approach their infinite separation limits as $1/d$ for large d; the dotted lines show such $1/d$ curves for each quantity matched to the $d/M = 50$ point.

using all three resolutions. For example, for the smallest separation $d = 1.56M$, we have $\max(|\Psi - 1|) = 0.05326$ (0.05325) and $\max|v| = 0.530149$ (0.530153) where the values in parentheses are the Richardson extrapolated quantities (which are consistent with approximately second-order convergence).

We can compare the above method of constructing free data for this case to a conformally flat method. Specifically, we set all the metric free data quantities to their flatspace values and set $\tilde{E}$ and $\tilde{p}^i$ for each star to a special-relativistically boosted density and pressure profile taken from the TOV solution. In Fig. 8 we show the same quantities as in Fig. 7 but using this conformally flat method. In this case the corrections from solving the constraints will not go to zero with infinite separation since all
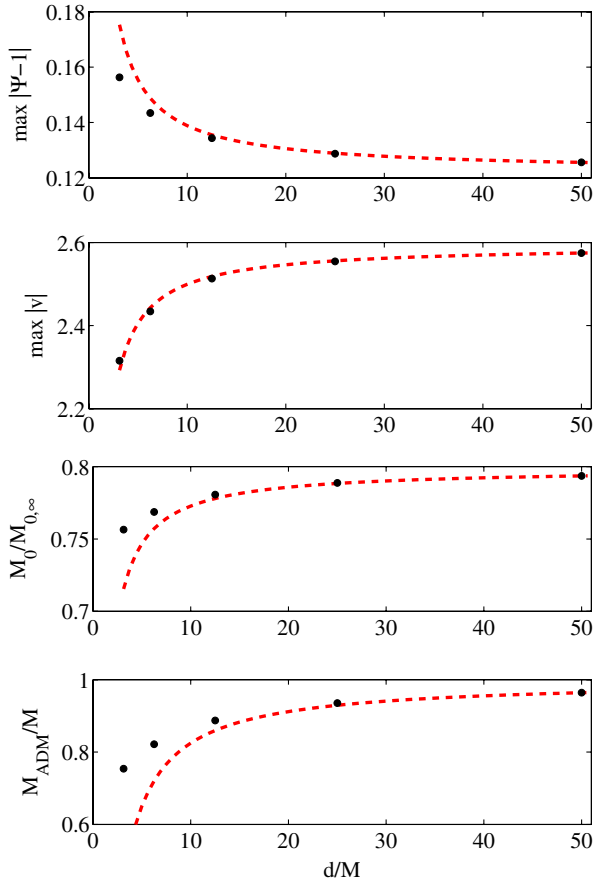
FIG. 8 (color online). Same as Fig. 7 but with conformally flat data. For all these cases the maximum of $|\Psi - 1|$ occurs for values of Ψ that are greater than unity.

the nontrivial geometry is coming from the conformal factor. Hence the energy momentum will be substantially rescaled at any separation. Also in contrast to the first method, the maximum of $|\Psi - 1|$ occurs for $\Psi > 1$ instead of $\Psi < 1$, which means E and p^i will be smaller than their conformal counterparts. With conformally flat ID it is also possible to solve for stars close together, though, as in the previous method, the ADM mass decreases steeply. It should also be noted that because of the large shift vector obtained with the second method, the coordinate velocity is substantially greater than one, which may make it more challenging to numerically evolve.

A full characterization of this ultrarelativistic collision ID requires evolution, which we present elsewhere [120].

IV. CONCLUSIONS

We have outlined a general method for constructing initial data based on superposition and the CTS formulation of the constraint equations, and demonstrated the method with some example solutions. Though there are numerous existing applications of the CTS method, and superposition has been proposed before, some of the notable aspects of the work presented here include adding

the matter and metric of neutron stars to the prescription, regularizing the interiors of black holes with (unphysical) matter sources, and applying it to regimes not yet studied before, namely, initial data for generic high-eccentricity binary mergers and ultrarelativistic collisions. For astrophysically relevant binaries we find that superposition of single, isolated compact object solutions works well in the sense that nonlinear correction from solving the constraints are relatively small for larger initial separations, implying that superposition is a good start to attain more astrophysically realistic initial data (for example, by adding prior gravitational wave information as in Ref. [82] to the superposed background data for quasicircular or low eccentricity inspirals). Including neutron stars, we find that the superposition effectively induces oscillations in the stars. This again is small for large separations and hence a good approximation to dynamical capture binaries. However, practical application to low eccentricity inspirals will likely require that the CTS equations be supplemented with some form of quasiequilibrium equations for the hydrodynamics (as in many existing ID methods, for example, Refs. [59,67,84]).

For the ultrarelativistic boost examples we are able to obtain solutions to the CTS equations with superposed and conformally flat data well into the kinetic energy dominated regime ($\gamma = 10$) for sufficiently large initial separations. At smaller separations we are still able to obtain solutions. However, for these initial data sets the corrections to the metric and fluid properties become large, and it is less clear how to separate the total energy of the spacetime into kinetic energy, rest-mass energy, etc. This will require evolution to resolve, and we leave that to future work. Nevertheless, given that there are few results on the uniqueness and existence of solutions to the conformal constraint equations beyond constant mean curvature slicing [121] (and in some cases, such as the extended CTS equations [122], there are known examples of nonuniqueness [123]), it is interesting that we are able to obtain solutions in this highly nonlinear regime.

ACKNOWLEDGMENTS

APPENDIX: MULTIGRID AMR INTERPOLATION

A multigrid algorithm requires a restriction operator to inject quantities from finer to coarser grids as well as a

prolongation operator to interpolate corrections from coarser grids to finer grids (see e.g., Ref. [124]). For our multigrid algorithm we use half-weight restriction as our restriction operator. In three dimensions half-weight restriction can be written as

$$f_{\text{HW}} = f_{i,j,k} + \frac{1}{12}(\Delta f_{xx} + \Delta f_{yy} + \Delta f_{zz}), \qquad \text{(A1)}$$

where

$$\Delta_{xx}f = f_{i+1,j,k} - 2f_{i,j,k} + f_{i-1,j,k}, \qquad \text{(A2)}$$

and similarly for the y and z directions. Note that $\Delta_{xx}f$ divided by h^2 (where h is the grid spacing) is a second-order approximation for $\partial_x^2 f$. On AMR boundaries where the full stencil is not available we must modify the above expression. For example, on a negative x boundary

we replace $\Delta_{xx}f$ by a right-handed second derivative stencil

$$\Delta_{xx}f = 2f_{i,j,k} - 5f_{i-1,j,k} + 4f_{i-2,j,k} - f_{i-3,j,k} \qquad \text{(A3)}$$

and so on for the other directions. This ensures not only that f_{HW} is a second-order representation of f, but also that f_{HW} is smooth to $O(h^4)$ on AMR boundaries. Hence if second derivatives of f_{HW} are computed including restricted boundary points in the stencil, the error will be $O(h^2)$.

We use linear interpolation as our prolongation operator. However, after applying a correction from a coarse grid, we reset the values on the AMR boundaries of the fine grid for the points that do not exist on the coarse level with fourth-order interpolation using those points that do. We found this higher order interpolation to be beneficial as we do not relax the points on the boundary.

[1] A. Abramovici *et al.*, Science **256**, 325 (1992).
[2] B. Caron *et al.*, Classical Quantum Gravity **14**, 1461 (1997).
[3] H. Lück *et al.*, Classical Quantum Gravity **14**, 1471 (1997).
[4] K. Somiya (LCGT Collaboration), Classical Quantum Gravity **29**, 124007 (2012).
[5] B. Sathyaprakash *et al.*, Classical Quantum Gravity **29**, 124013 (2012).
[6] H. P. Pfeiffer, Classical Quantum Gravity **29**, 124004 (2012).
[7] F. Pretorius, in *Physics of Relativistic Objects in Compact Binaries: From Birth to Coalescence*, edited by M. Colpi, P. Casella, V. Gorini, U. Moschella, and A. Possenti (Springer, Netherlands, 2009), Vol. 359, pp. 305–369.
[8] M. Hannam, Classical Quantum Gravity **26**, 114001 (2009).
[9] J. Centrella, J. G. Baker, B. J. Kelly, and J. R. van Meter, Rev. Mod. Phys. **82**, 3069 (2010).
[10] S. T. McWilliams, Classical Quantum Gravity **28**, 134001 (2011).
[11] J. A. Faber and F. A. Rasio, Living Rev. Relativity **15**, 8, (2012).
[12] M. Shibata and K. Taniguchi, Living Rev. Relativity **14**, 6, (2011).
[13] M. D. Duez, Classical Quantum Gravity **27**, 114002 (2010).
[14] I. Hinder, F. Herrmann, P. Laguna, and D. Shoemaker, Phys. Rev. D **82**, 024033 (2010).
[15] J. Healy, F. Herrmann, I. Hinder, D. M. Shoemaker, P. Laguna, and R. A. Matzner, Phys. Rev. Lett. **102**, 041101 (2009).
[16] B. C. Stephens, W. E. East, and F. Pretorius, Astrophys. J. **737**, L5 (2011).
[17] W. E. East, F. Pretorius, and B. C. Stephens, Phys. Rev. D **85**, 124009 (2012).
[18] R. Gold, S. Bernuzzi, M. Thierfelder, B. Bruegmann, and F. Pretorius, arXiv:1109.5128.

[19] U. Sperhake, E. Berti, V. Cardoso, J. A. González, B. Brügmann, and M. Ansorg, Phys. Rev. D **78**, 064069 (2008).
[20] F. Pretorius and D. Khurana, Classical Quantum Gravity **24**, S83 (2007).
[21] M. C. Washik, J. Healy, F. Herrmann, I. Hinder, D. Shoemaker, P. Laguna, and R. Matzner, Phys. Rev. Lett. **101**, 061102 (2008).
[22] I. Hinder, B. Vaishnav, F. Herrmann, D. M. Shoemaker, and P. Laguna, Phys. Rev. D **77**, 081502 (2008).
[23] R. Gold, S. Bernuzzi, M. Thierfelder, B. Bruegmann, and F. Pretorius, arXiv:1109.5128.
[24] R. Gold and B. Bruegmann, arXiv:1209.4085.
[25] C. D. Ott, Classical Quantum Gravity **26**, 063001 (2009).
[26] C. L. Fryer and K. C. New, Living Rev. Relativity **14**, 1, (2011).
[27] J. A. Font, Living Rev. Relativity **11**, 7, (2008).
[28] B. K. Berger, Living Rev. Relativity **5**, 1, (2002).
[29] D. Garrison, arXiv:1207.7097.
[30] V. e. a. Cardoso, arXiv:1201.5118.
[31] C. Gundlach and J. M. Martin-Garcia, Living Rev. Relativity **10**, 5, (2007).
[32] U. Sperhake, V. Cardoso, F. Pretorius, E. Berti, and J. A. Gonzalez, Phys. Rev. Lett. **101**, 161101 (2008).
[33] M. Shibata, H. Okawa, and T. Yamamoto, Phys. Rev. D **78**, 101501 (2008).
[34] M. W. Choptuik and F. Pretorius, Phys. Rev. Lett. **104**, 111101 (2010).
[35] H. Okawa, K.-i. Nakao, and M. Shibata, Phys. Rev. D **83**, 121501 (2011).
[36] H. Witek, V. Cardoso, L. Gualtieri, C. Herdeiro, U. Sperhake, and M. Zilhão, Phys. Rev. D **83**, 044017 (2011).
[37] P. M. Chesler and L. G. Yaffe, Phys. Rev. Lett. **102**, 211601 (2009).
[38] P. M. Chesler and L. G. Yaffe, Phys. Rev. Lett. **106**, 021601 (2011).

[39] P. M. Chesler and D. Teaney, arXiv:1112.6196.

[40] H. Bantilan, F. Pretorius, and S. S. Gubser, Phys. Rev. D **85**, 084038 (2012).

[41] A. Buchel, L. Lehner, and R. C. Myers, J. High Energy Phys. 08 (2012) 049.

[42] T. Wiseman, *Black Holes in Higher Dimensions*, edited by G. T. Horowitz, (Cambridge Unviersity Press, Cambridge, England, 2012).

[43] M. Shibata and H. Yoshino, Phys. Rev. D **81**, 021501 (2010).

[44] L. Lehner and F. Pretorius, Phys. Rev. Lett. **105**, 101102 (2010).

[45] P. Bizon and A. Rostworowski, Phys. Rev. Lett. **107**, 031102 (2011).

[46] J. W. York, Phys. Rev. Lett. **82**, 1350 (1999).

[47] J. W. York, Jr., *Initial Data for Collisions of Black Holes and Other Gravitational Miscellany* (Cambridge Unviersity Press, Cambridge, England, 1989), pp. 89–109.

[48] G. B. Cook, Living Rev. Relativity **3**, 5, (2000).

[49] H. P. Pfeiffer, arXiv:gr-qc/0412002.

[50] E. Gourgoulhon, J. Phys. Conf. Ser. **91**, 012001 (2007).

[51] J. M. Bowen and J. W. York, Jr., Phys. Rev. D **21**, 2047 (1980).

[52] A. Garat and R. H. Price, Phys. Rev. D **61**, 124011 (2000).

[53] G. B. Cook and J. W. York, Jr., Phys. Rev. D **41**, 1077 (1990).

[54] G. Lovelace, R. Owen, H. P. Pfeiffer, and T. Chu, Phys. Rev. D **78**, 084017 (2008).

[55] G. B. Cook, M. Choptuik, M. Dubal, S. Klasky, R. Matzner, and S. Oliveira, Phys. Rev. D **47**, 1471 (1993).

[56] G. B. Cook, Phys. Rev. D **50**, 5025 (1994).

[57] J. R. Wilson, G. J. Mathews, and P. Marronetti, Phys. Rev. D **54**, 1317 (1996).

[58] T. W. Baumgarte, G. B. Cook, M. A. Scheel, S. L. Shapiro, and S. A. Teukolsky, Phys. Rev. Lett. **79**, 1182 (1997).

[59] S. Bonazzola, E. Gourgoulhon, and J.-A. Marck, Phys. Rev. D **56**, 7740 (1997).

[60] G. B. Cook, Phys. Rev. D **65**, 084003 (2002).

[61] E. Gourgoulhon, P. Grandclément, and S. Bonazzola, Phys. Rev. D **65**, 044020 (2002).

[62] P. Grandclément, E. Gourgoulhon, and S. Bonazzola, Phys. Rev. D **65**, 044021 (2002).

[63] W. Tichy and B. Bruegmann, Phys. Rev. D **69**, 024006 (2004).

[64] G. B. Cook and H. P. Pfeiffer, Phys. Rev. D **70**, 104016 (2004).

[65] M. Ansorg, B. Bruegmann, and W. Tichy, Phys. Rev. D **70**, 064011 (2004).

[66] M. Ansorg, Phys. Rev. D **72**, 024018 (2005).

[67] M. Shibata, K. Uryū, and J. L. Friedman, Phys. Rev. D **70**, 044044 (2004).

[68] P. Grandclément, Phys. Rev. D **74**, 124002 (2006).

[69] F. Foucart, L. E. Kidder, H. P. Pfeiffer, and S. A. Teukolsky, Phys. Rev. D **77**, 124051 (2008).

[70] K. Taniguchi, T. W. Baumgarte, J. A. Faber, and S. L. Shapiro, Phys. Rev. D **74**, 041502 (2006).

[71] J. D. Grigsby and G. B. Cook, Phys. Rev. D **77**, 044011 (2008).

[72] H. P. Pfeiffer, G. B. Cook, and S. A. Teukolsky, Phys. Rev. D **66**, 024047 (2002).

[73] M. Hannam, S. Husa, B. Bruegmann, J. A. Gonzalez, and U. Sperhake, Classical Quantum Gravity **24**, S15 (2007).

[74] R. A. Matzner, M. F. Huq, and D. Shoemaker, Phys. Rev. D **59**, 024015 (1998).

[75] P. Marronetti and R. A. Matzner, Phys. Rev. Lett. **85**, 5500 (2000).

[76] G. Lovelace, Classical Quantum Gravity **26**, 114002 (2009).

[77] Y. T. Liu, Z. B. Etienne, and S. L. Shapiro, Phys. Rev. D **80**, 121503 (2009).

[78] W. Tichy, B. Brügmann, M. Campanelli, and P. Diener, Phys. Rev. D **67**, 064008 (2003).

[79] S. Nissanke, Phys. Rev. D **73**, 124002 (2006).

[80] N. Yunes, W. Tichy, B. J. Owen, and B. Bruegmann, Phys. Rev. D **74**, 104011 (2006).

[81] N. K. Johnson-McDaniel, N. Yunes, W. Tichy, and B. J. Owen, Phys. Rev. D **80**, 124039 (2009).

[82] G. Reifenberger and W. Tichy, Phys. Rev. D **86**, 064003 (2012).

[83] G. Lovelace, M. A. Scheel, and B. Szilágyi, Phys. Rev. D **83**, 024010 (2011).

[84] M. Shibata, K. Uryū, and J. L. Friedman, Phys. Rev. D **70**, 129901 (2004).

[85] K. Uryu, F. Limousin, J. L. Friedman, E. Gourgoulhon, and M. Shibata, Phys. Rev. Lett. **97**, 171101 (2006).

[86] G. B. Cook and T. W. Baumgarte, Phys. Rev. D **78**, 104016 (2008).

[87] K. Uryū, F. Limousin, J. L. Friedman, E. Gourgoulhon, and M. Shibata, Phys. Rev. D **80**, 124004 (2009).

[88] M. Hannam, S. Husa, D. Pollney, B. Brügmann, and N. O. Murchadha, Phys. Rev. Lett. **99**, 241102 (2007).

[89] M. Hannam, S. Husa, F. Ohme, B. Brügmann, and N. Ó Murchadha, Phys. Rev. D **78**, 064020 (2008).

[90] M. Hannam, S. Husa, and N. O. Murchadha, Phys. Rev. D **80**, 124007 (2009).

[91] J. D. Immerman and T. W. Baumgarte, Phys. Rev. D **80**, 061501 (2009).

[92] S. Brandt and B. Bruegmann, Phys. Rev. Lett. **78**, 3606 (1997).

[93] T. W. Baumgarte, Phys. Rev. D **85**, 084013 (2012).

[94] A. Arbona, C. Bona, J. Carot, L. Mas, J. Massó, and J. Stela, Phys. Rev. D **57**, 2397 (1998).

[95] D. Brown, O. Sarbach, E. Schnetter, M. Tiglio, P. Diener, I. Hawke, and D. Pollney, Phys. Rev. D **76**, 081503 (2007).

[96] D. Brown, P. Diener, O. Sarbach, E. Schnetter, and M. Tiglio, Phys. Rev. D **79**, 044023 (2009).

[97] M. H. P. M. van Putten, Phys. Rev. D **54**, R5931 (1996).

[98] P. Marronetti, M. Huq, P. Laguna, L. Lehner, R. Matzner, and D. Shoemaker, Phys. Rev. D **62**, 024017 (2000).

[99] G. B. Cook and M. A. Scheel, Phys. Rev. D **56**, 4775 (1997).

[100] F. Pretorius and M. W. Choptuik, J. Comput. Phys. **218**, 246 (2006).

[101] M. Alcubierre, B. Brügmann, D. Holz, R. Takahashi, S. Brandt, E. Seidel, and J. Thornburg, Int. J. Mod. Phys. D **10**, 273 (2001).

[102] F. Pretorius, Classical Quantum Gravity **22**, 425 (2005).

[103] W. E. East, F. Pretorius, and B. C. Stephens, Phys. Rev. D **85**, 124010 (2012).

[104] H. P. Pfeiffer, D. A Brown, L. E Kidder, L. Lindblom, G. Lovelace, and M. A Scheel, Classical Quantum Gravity **24**, S59 (2007).

[105] S. Husa, M. Hannam, J. A. González, U. Sperhake, and B. Brügmann, Phys. Rev. D **77**, 044037 (2008).

[106] M. A. Scheel, M. Boyle, T. Chu, L. E. Kidder, K. D. Matthews, and H. P. Pfeiffer, Phys. Rev. D **79**, 024003 (2009).

[107] J. S. Read, C. Markakis, M. Shibata, K. Uryū, J. Creighton, and J. Friedman, Phys. Rev. D **79**, 124033 (2009).

[108] G. 't Hooft, Phys. Lett. B **198**, 61 (1987).

[109] T. Banks and W. Fischler, arXiv:hep-th/9906038.

[110] E. Kohlprath and G. Veneziano, J. High Energy Phys. 6 (2002) 057.

[111] K. S. Thorne, in *Magic Without Magic: John Archibald Wheeler*, edited by J. Klauder (Freeman, San Francisco, 1972), p. 231.

[112] N. Arkani-Hamed, S. Dimopoulos, and G. Dvali, Phys. Lett. B **429**, 263 (1998).

[113] L. Randall and R. Sundrum, Phys. Rev. Lett. **83**, 3370 (1999).

[114] S. Dimopoulos and G. Landsberg, Phys. Rev. Lett. **87**, 161602 (2001).

[115] S. B. Giddings and S. Thomas, Phys. Rev. D **65**, 056010 (2002).

[116] J. L. Feng and A. D. Shapere, Phys. Rev. Lett. **88**, 021303 (2001).

[117] C. de los Heros, arXiv:astro-ph/0701333.

[118] S. Chatrchyan *et al.* (CMS Collaboration), J. High Energy Phys. 04 (2012) 061.

[119] P. C. Aichelburg and R. U. Sexl, Gen. Relativ. Gravit. **2**, 303 (1971).

[120] W. E. East and F. Pretorius, arXiv:1210.0443.

[121] A. Rendall, Living Rev. Relativity **5**, 6 (2002).

[122] H. P. Pfeiffer and J. W. York, Phys. Rev. D **67**, 044022 (2003).

[123] H. P. Pfeiffer and J. W. York, Phys. Rev. Lett. **95**, 091101 (2005).

[124] W. H. Press, S. A. Teukolsky, W. T. Vetterling, and B. P. Flannery, *Numerical Recipes: The Art of Scientific Computing* (Cambridge University Press, Cambridge, U.K., 2007), 3rd ed.